Click Here for Full Article

Phytoplankton scales of variability in the California Current System: 2. Latitudinal variability

Stephanie A. Henson[1] and Andrew C. Thomas[1]

[1]   The California Current System encompasses a southward flowing current which is perturbed by ubiquitous mesoscale variability. The extent to which latitudinal patterns of physical variability are reflected in the distribution of biological parameters is poorly known. To investigate the latitudinal distribution of chlorophyll variance, a wavelet analysis is applied to nearly 9 years (October 1997 to July 2006) of 1-km-resolution Sea-viewing Wide Field-of-view Sensor (SeaWiFS) chlorophyll concentration data at 5-day resolution. Peaks in the latitudinal distribution of chlorophyll variance coincide with features of the coastal topography. Maxima in variance are located offshore of Vancouver Island and downstream of Heceta Bank, Cape Blanco, Point Arena, and possibly Point Conception. An analysis of dominant wavelengths in the chlorophyll data reveals a transfer of energy into smaller scales is generated in the vicinity of the coastal capes. The latitudinal distribution of variance in sea level anomaly corresponds closely to the chlorophyll variance in the nearshore region (<100 km offshore), suggesting that the same processes determine the distribution of both. Farther offshore, there is no correspondence between latitudinal patterns of sea level anomaly and chlorophyll variance. This likely represents a transition from physical to biological control of the phytoplankton distribution.

1.   Introduction

[2]   The California Current System (CCS) is an eastern boundary flow extending from the bifurcation of the West Wind Drift at ∼50°N to Baja California. Seasonally varying equatorward winds result in vigorous coastal upwelling and a predominantly southward surface flow [*Hickey*, 1998]. The equatorward current develops meanders, filaments and eddies, evident in satellite imagery of sea surface temperature (SST) and phytoplankton pigment [e.g., *Traganza et al.*, 1980; *Ikeda et al.*, 1984a, 1984b; *Ramp et al.*, 1991; *Abbott and Barksdale*, 1991]. The structures observed in SST and Coastal Zone Color Scanner (CZCS) data correspond closely, implying that physical processes are important to phytoplankton distribution in this region [*Abbott and Zion*, 1985; *Denman and Abbott*, 1994]. In the CCS the role of mesoscale variability in several biological processes has been demonstrated, for example, delivery of nutrients [*Chavez et al.*, 1991], offshore transport of phytoplankton [*Washburn et al.*, 1991] and zooplankton community composition and distribution [*Mackas et al.*, 1991].

[3]   The location of persistent meanders and filaments in the southward flowing jet are often associated with the coastal topography. From Washington to Point Conception (∼34°N–48°N) the coastline is aligned almost north-south

but several capes protrude from the coast, deflecting the jet offshore. The flow-topography interaction results in increased mesoscale variability in the vicinity of the capes [e.g., *Ikeda and Emery*, 1984a; *Haidvogel et al.*, 1991; *Batteen et al.*, 2003; *Marchesiello et al.*, 2003; *Castelao and Barth*, 2005] and enhanced biomass in the lee of the capes has also been observed [*Barth et al.*, 2005; *Huyer et al.*, 2005].

[4]   Satellite data are well suited to the task of assessing phytoplankton variability, as it provides repeated, synoptic imagery over large spatial and temporal scales. To extract the dominant modes of variability we employ the method of wavelet analysis, which decomposes a signal into time-frequency, or distance-wavelength, space. In a companion paper [*Henson and Thomas*, 2007] (hereinafter HT07) a detailed description of the wavelet transform is given, with a focus on interpreting the results of an analysis. HT07 quantifies the dominant temporal scales of phytoplankton variability in SeaWiFS chlorophyll concentration (chl *a*) data as a function of cross-shelf distance using latitudinal means of the entire study region and identifies their seasonal and interannual variability. Maximum variance in chlorophyll was found to have a period of ∼100–200 days. The timing of peak variance varied seasonally with cross-shelf distance, with maxima in spring/summer close to shore and in autumn/winter offshore, consistent with the seasonal offshore migration of the coastal jet. Substantial interannual variability in the magnitude of chlorophyll variance was also observed and found to be strongly out of phase with the

---

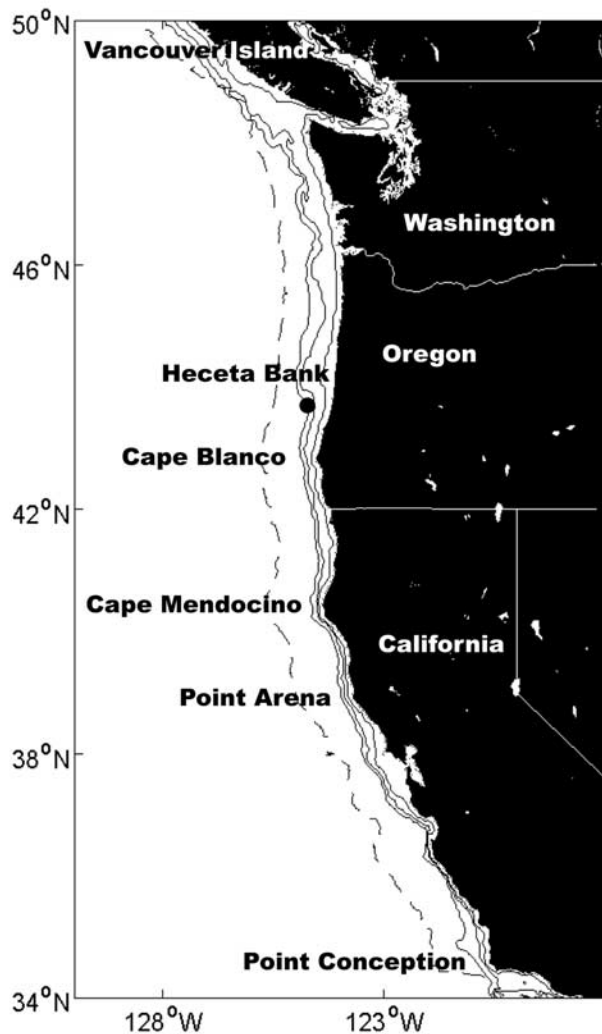[1]School of Marine Sciences, University of Maine, Orono, Maine, USA.

Figure 1. Map of the study region showing bathymetric contours at 50, 200, and 500 m depth. The dashed line shows the location of the 100-km offshore transect. Black dot marks position of example time series in Figure 2a. Locations mentioned in the text are labeled.

Pacific Decadal Oscillation index. In this paper we apply wavelet analysis to the same SeaWiFS chl *a* data set as in HT07 to assess the latitudinal distribution of chlorophyll variance.

2. Data

[5] Daily SeaWiFS chlorophyll *a* (chl *a*) concentration data at 1 km resolution were downloaded from the NASA Ocean Color Browser (http://oceancolor.gsfc.nasa.gov/). All level 2 MLAC files (v5.1 reprocessing) from 2 October 1997 to 31 July 2006 in the boundaries 34°N–50°N, 130°W–118°W (Figure 1) were downloaded. Individual passes were remapped to a cylindrical projection and multiple passes on a calendar day were composited. On average ~20% of the data were missing owing to cloudiness, and therefore daily images were then composited into 5-day means to reduce gaps. Any gaps shorter than three

time steps (i.e., 15 days) in length were filled by linear interpolation in time. Remaining gaps were filled with a mean value, calculated for that pixel and 5-day period from all valid data in other years. The climatological mean seasonal cycle, calculated at each pixel, was removed from the data prior to performing wavelet analysis. The resulting time series were subsampled as transects parallel to the coast at distances 20, 50, 100 and 200 km offshore (Figure 1).

[6] Multimission (JASON and TOPEX/POSEIDON) gridded SLA data at 7-day, 0.25° resolution from October 1997 to July 2006 were obtained from http://www.aviso. oceanobs.com. The climatological seasonal cycle was removed from the data prior to analysis. Transects parallel to the coast were extracted at the same locations as the chl *a* data. In the transect closest to shore, data are absent between 41°N and 42°N owing to land detection errors in the AVISO data set.

[7] We briefly illustrate the wavelet analysis method using an example time series of SeaWiFS chl *a* data at 43.8°N, 124.8°W. Further details of the method used are given by HT07 and formal mathematical descriptions by *Morlet* [1983] or *Daubechies* [1992]. A Morlet-6 wavelet transform was applied to the time series (Figure 2a). The resulting local wavelet power spectrum (Figure 2b) describes the relative amplitude of features at a particular frequency and time. The contours represent wavelet power and can be interpreted as a 'map' of the time variability of dominant frequencies. The unit of wavelet power is the original data unit squared, i.e., the variance (in the case of chl *a* this is $(mg\ m^{-3})^2$). Thick solid lines denote the 95% confidence level, assuming a white-noise background spectrum [*Torrence and Compo*, 1998]. Errors increase at the edges of the wavelet spectrum owing to the finite length of the time series, and data below the cone of influence (thin solid line in Figure 2b) should be regarded with caution. In this example, the largest peak in wavelet power occurs in 2002 with dominant periods of ~70–150 days. Smaller peaks occur in 1998, 2003, 2004 and 2005 with periods of ~80–120 days, and relatively weak wavelet power is evident only at periods greater than ~200 days in 1999 and 2000.

[8] The information contained in the local wavelet spectrum can be summarized by the global wavelet power spectrum (GWPS; Figure 2c) and scale-averaged time series (Figure 2d). The GWPS is the time-averaged wavelet power at each period and in this example has a peak at periods ~100 days (Figure 2c). The scale-averaged time series is the mean variance contained in a certain period band. Averaging over the period band 80–120 days (Figure 2d) indicates that maximum variance occurs throughout 2002 and in 2005. In 1999 and 2000 variance in this period band is below the 95% confidence level.

3. Results

[9] At each pixel along a transect (1 km spacing) a wavelet analysis was performed on the time series of data. The resulting local wavelet power spectra were scale-averaged over a period band of ~100–200 days (as in Figure 2d), the range of periods in which peak chl *a* is generally observed (HT07). The scale-averaged time series for each transect (20, 50, 100 and 200 km offshore) are then
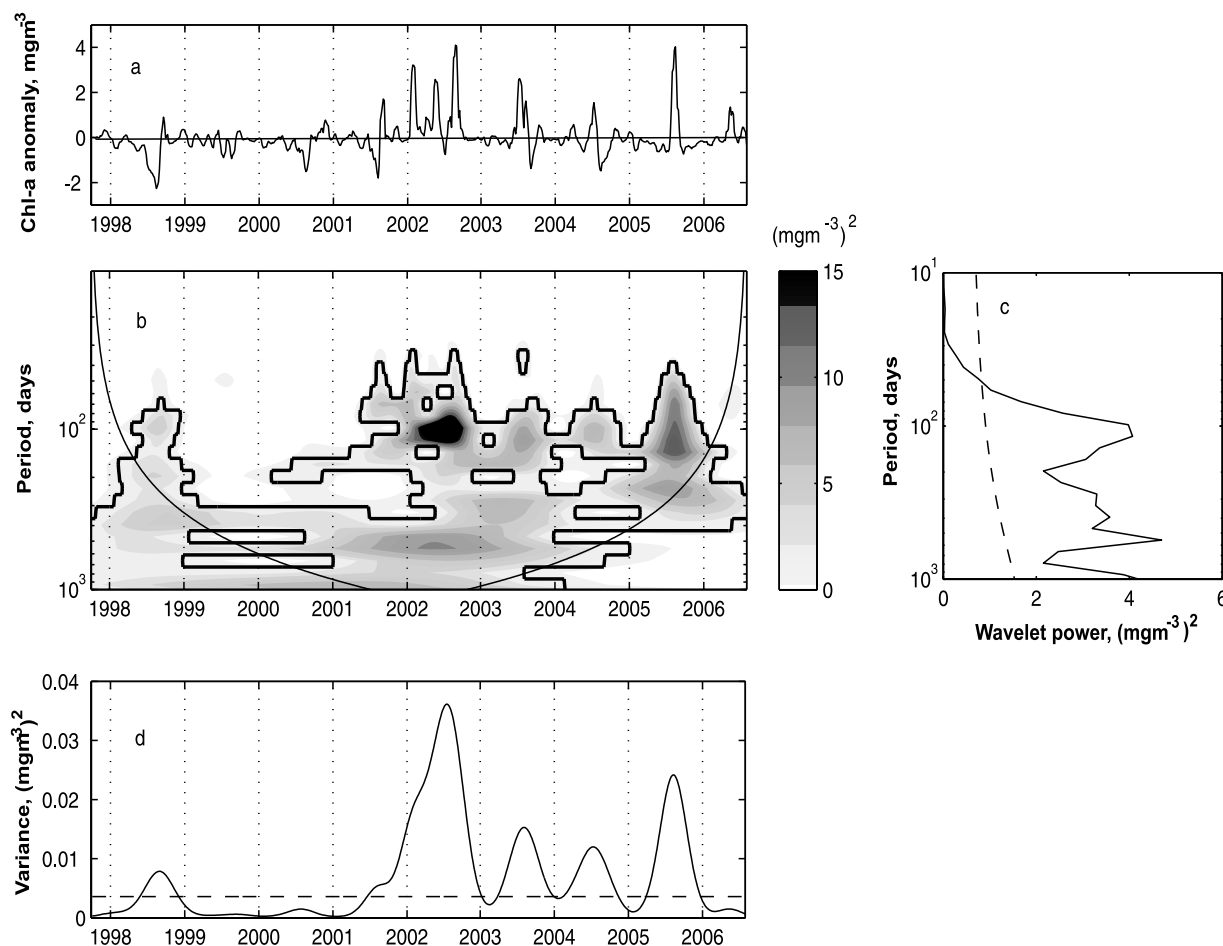
Figure 2. (a) Time series of SeaWiFS chl *a* anomalies at 43.8°N, 124.8°W. (b) Local wavelet power spectrum of the time series. High values of wavelet power indicate frequencies and times at which chl *a* variance is high. Thick black line is the 95% confidence level. Thin line is the cone of influence, below which edge effects become important. The *y* axis has been converted from wavelet scale, *a*, to frequency. For the Morlet-6 wavelet, frequency = 1.03*a* [*Torrence and Compo*, 1998]. The smallest scale resolved is at the Nyquist frequency (∼10 days). (c) Global wavelet power spectrum, i.e., the temporal mean wavelet power at each period. Dashed line is the 95% confidence level. (d) Scale-averaged time series for the period band 80–120 days. Wavelet power has been normalized by $N/2\sigma^2$ (where N is the number of data points and σ^2 is its variance). Dashed line is the 95% confidence level.

combined into a two-dimensional view of the temporal and spatial variability of chl *a* variance in this particular period band (contour plots in Figures 3a–3d), known as 'power Hovmöller' plots [*Torrence and Compo*, 1998]. Thick black lines enclose regions with >95% confidence. In this paper our focus is on the latitudinal distribution of chl *a* variance. The interannual variability is discussed in HT07. Line plots in Figures 3e–3h show the latitudinal distribution of the time averaged variance in chl *a* at periods of 100–200 days.

[10] At each distance offshore, maximum variance occurs between 46°N–50°N (in the vicinity of Vancouver Island) and 36°N–38°N (south of Point Arena). High variance occurs consistently every year north of ∼48°N, but is more patchy farther south. At 20 km offshore, maxima in chl *a* variance occur at 46°N–50°N and 36°N–39°N (Figure 3a). Peaks in variance in the north occur consistently in all years (although in 2000 variance is particularly weak). The time mean variance (Figure 3e) has peaks at 46°N–50°N, 44°N

(near Heceta Bank), 43°N (in the vicinity of Cape Blanco), 40°N–41.5°N (near Cape Mendocino), 36°N–39°N and 35°N (north of Point Conception). At a distance of 50 km offshore, the time mean variance (Figure 3f) has broad peaks at 46°N–50°N, 40°N–42°N and 36°N–38°N. A localized maximum occurs at 44°N. At 100 km offshore, the time mean variance (Figure 3g) has a broad peak between 47°N and 50°N and smaller maxima at 45°N, 44°N and 43°N. Another broad peak occurs at 40°N°42°N and 36°N–38°N. At 200 km offshore, largest peaks in the time mean chl *a* variance (Figure 3h) occur at 36°N–38°N and 48°N. Smaller peaks are regularly spaced (∼150 km apart) between 38°N and 47°N.

[11] A clear structure is observed in the latitudinal distribution of chl *a* variance. However, the plots in Figure 3 are only for the period band 100–200 days. It is fair to ask whether locations with low chl *a* variance in the 100- to 200-day band are characterized by low variance in general, or whether peak wavelet power is shifted into different
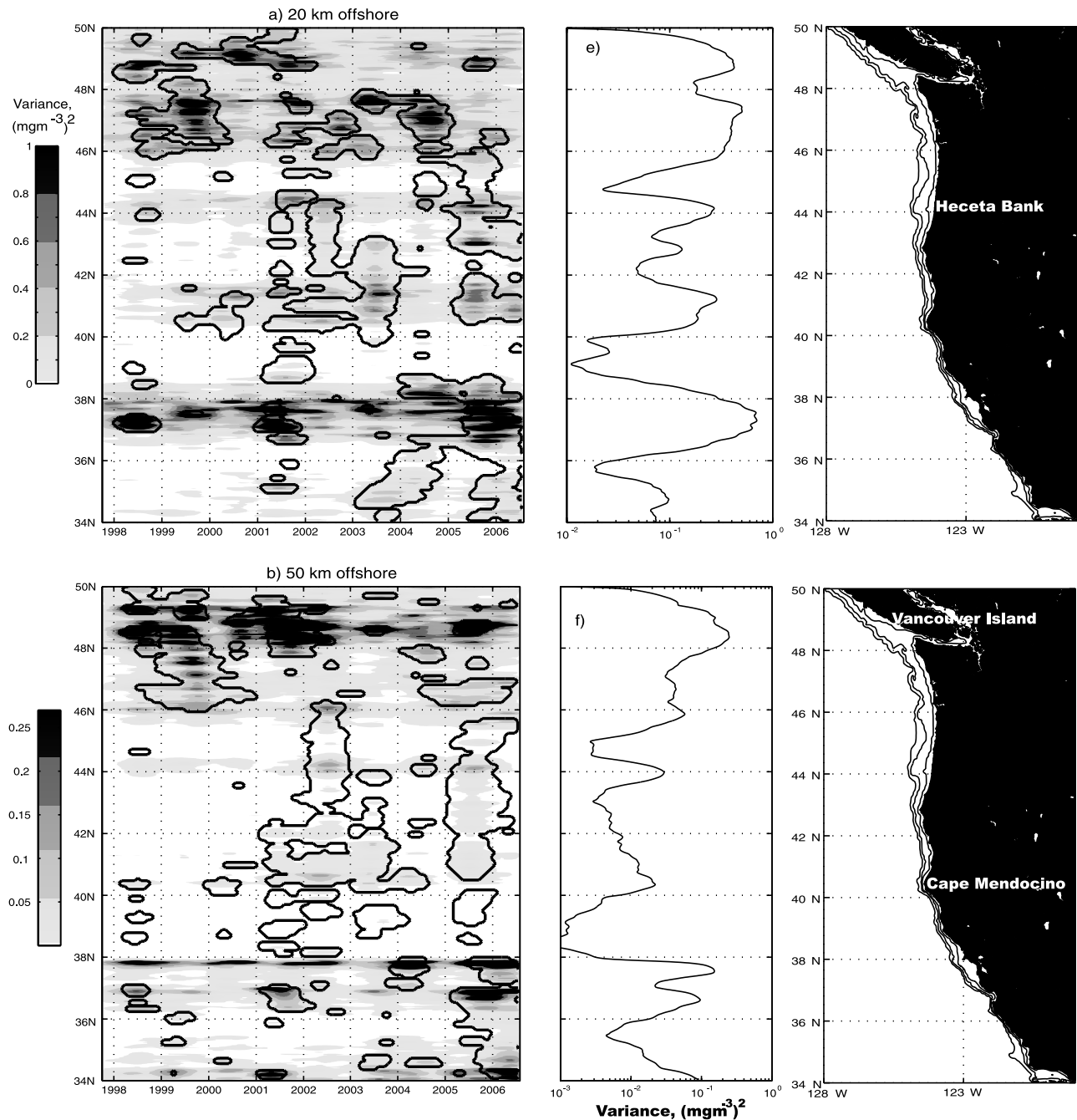
Figure 3. Power Hovmöller plots for scale-averaged (period band ∼100−200 days) chl *a* wavelet power for transects taken (a) 20 km offshore, (b) 50 km offshore, (c) 100 km offshore, and (d) 200 km offshore. Thick black line indicates the 95% confidence level. Time-averaged power spectra for period band ∼100−200 days as a function of latitude for transects (e) 20 km offshore, (f) 50 km offshore, (g) 100 km offshore, and (h) 200 km offshore. Maps of study region show bathymetric contours at 50, 200, and 500 m depth. Locations mentioned in text are labeled.

periods and therefore not represented in Figure 3. The latitudinal distribution of wavelet power in multiple period bands can be assessed using the global wavelet power spectrum (as in Figure 2c). At each point in a transect the wavelet transform is applied to the time series of chl *a* data. The resulting global spectra (and 95% confidence level) are contoured as a function of latitude in Figure 4. Note that although a particular period or location may not contain any

statistically significant wavelet power globally (i.e., averaged over all time), it may still have significant local power (i.e., at a particular point in time), and vice versa. In Figure 4 vertically oriented structure indicates coherence across period bands. At 20 km offshore, wavelet power occurs at a wide range of periods at most latitudes. Drops in power occur at all periods at ∼45°N, 43°N, 39°N and 36°N. At 50 km offshore statistically significant wavelet power

Figure 3. (continued)
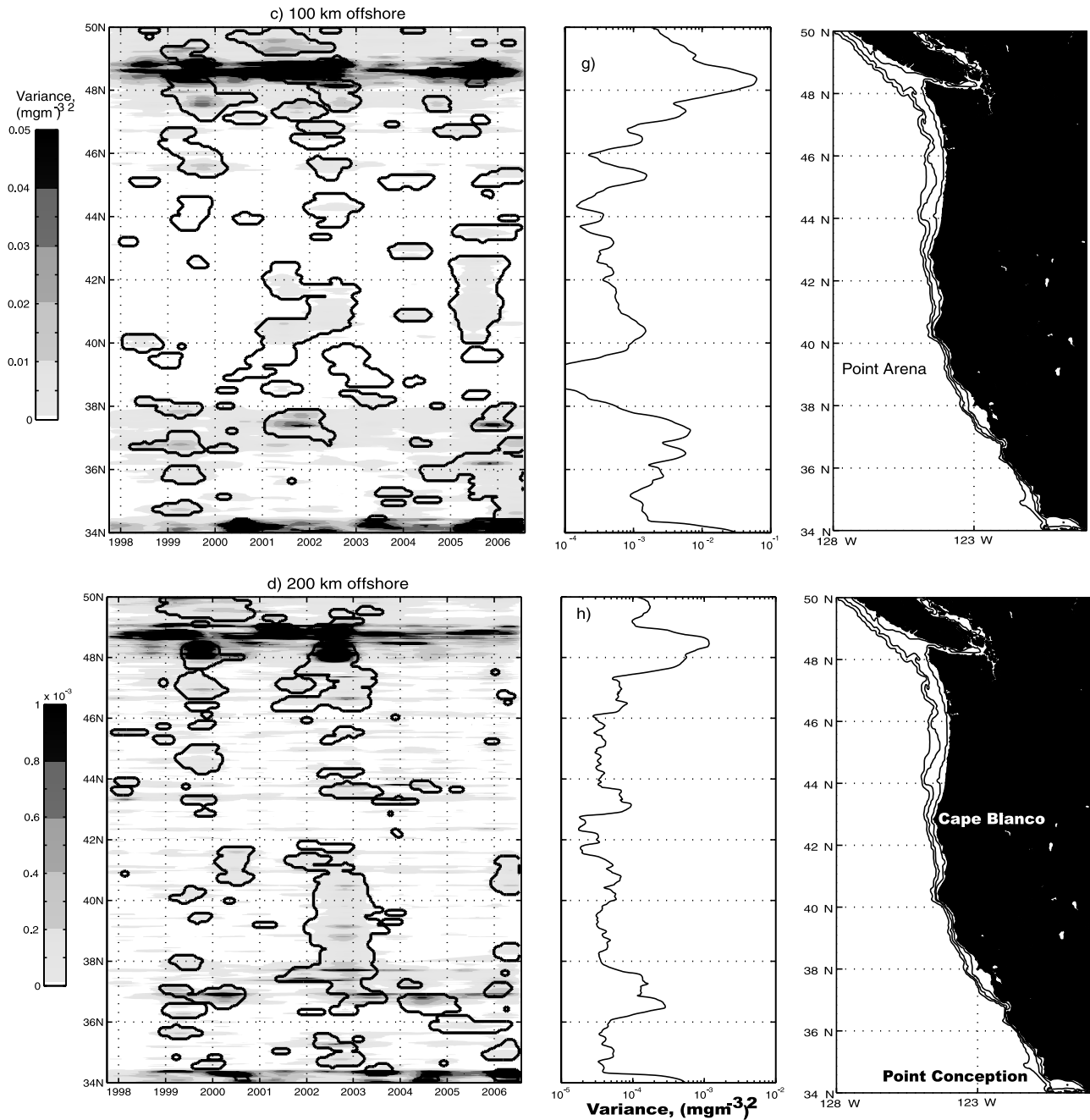
occurs at a large range of periods only between ∼46°N–50°N and 34°N–38°N. Statistically significant power occurs only at periods ∼50–400 days between ∼40°N and 43°N. At 45°N and 38°N–40°N there is very little statistically significant wavelet power at any period. One hundred kilometers offshore high, statistically significant wavelet power occurs from ∼20 to 400 days at ∼48°N–50°N and 34°N. Apart from these two areas statistically significant wavelet power is scarce, with only small patches, principally ∼37°N–38°N. By 200 km offshore statistically significant wavelet power is very sparse with the only spatially coherent area occurring ∼48°N–50°N. At each distance from shore, Figure 4 demonstrates that maxima and minima in variance are strongly coherent across period

bands at each latitude. At locations where chl *a* variance is low in the 100- to 200-day period band, wavelet power is generally low at all periods, and is not simply shifted into different periods.

[12] To investigate the latitudinal distribution of the wavelengths (rather than periods) of chl *a* variance we employed a spatial wavelet analysis (all results so far have been from a temporal analysis). The resulting wavelet power spectra are a function of distance and wavelength (rather than time and period). For each location 20, 50, 100 and 200 km offshore a wavelet analysis was performed on a time-averaged transect of chl *a*. From the resulting local wavelet power spectra, the shortest statistically significant
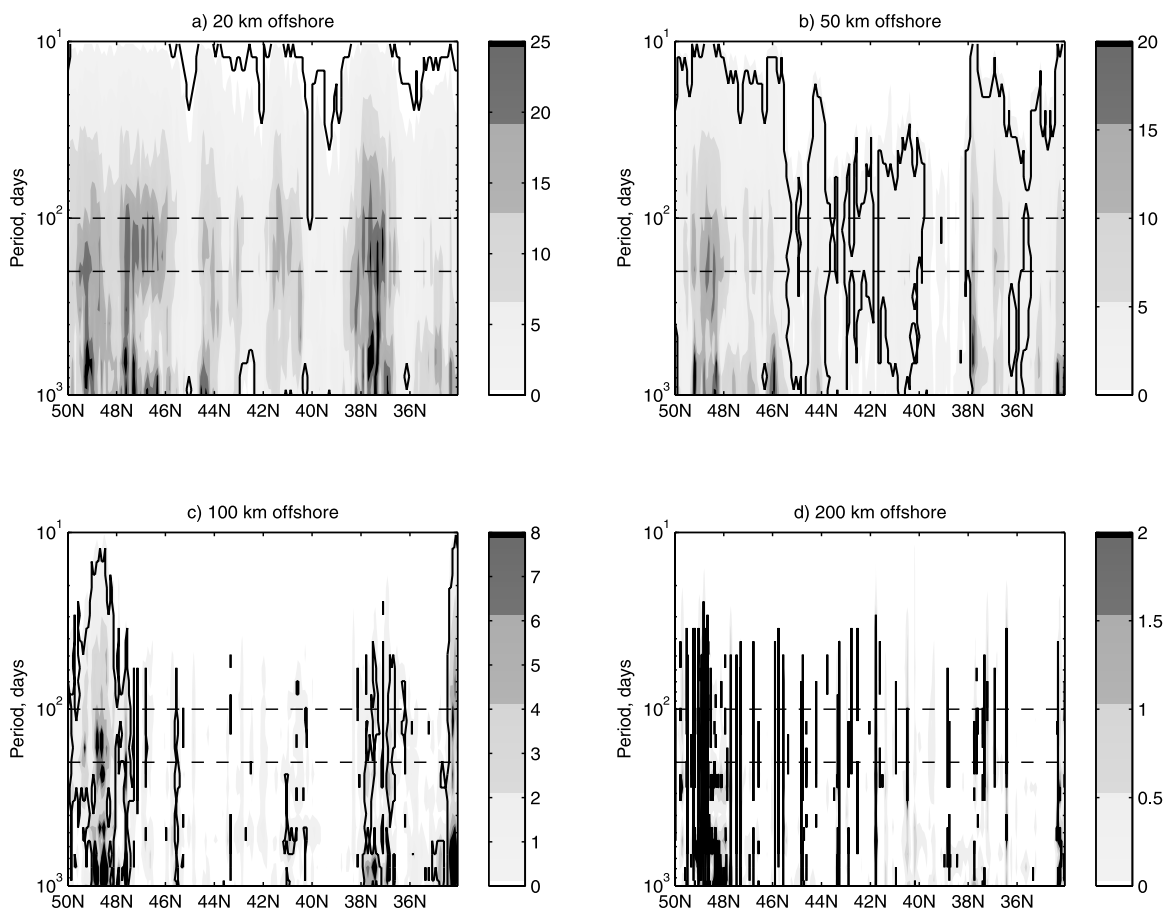
Figure 4. Global wavelet power spectra (mg m^{-3})^2 at (a) 20 km, (b) 50 km, (c) 100 km, and (d) 200 km offshore. Solid contour is the 95% confidence level. Dashed lines mark periods of 100 and 200 days.

(95% confidence level) wavelength at each latitude was extracted (Figure 5).

[13] Overall there is a progression of increasing wavelength with increasing distance from shore. At 20 km offshore, the shortest significant wavelengths vary from ~40 km, shortening to ~10−20 km at ~46°N−50°N, 44°N, 41.5°N and 37°N−38°N. At 50 km offshore wavelengths shorten from ~60 km to ~5−20 km at 48°N−50°N, 44°N and 34°N−38°N. At 100 km offshore wavelengths shorten from ~70 km to ~5−10 km at 47°N−50°N, and to ~20−30 km at 41°N and 36°N−38°N. At 200 km offshore wavelengths shorten from ~80 km to ~5−20 km at 47°N−50°N, 43°N−44°N and 36°N−38°N and to ~30 km at 41°N. Many of the short-wavelength peaks in Figure 5 correspond in latitude to maxima in chl a variance (Figures 3e−3h), suggesting that at these locations not only is chl a variance increased, but it is also dominated by smaller mesoscale features.

4. Discussion

4.1. Latitudinal Variability

[14] In the California Current System an equatorward surface current develops annually in spring [*Hickey*, 1979]. The many capes and offshore extensions of bottom topography in Oregon and northern California perturb the southward flow, causing meanders and mesoscale features

to develop in the coastal jet [*Ikeda and Emery*, 1984a, 1984b; *Haidvogel et al.*, 1991; *Barth et al.*, 2005]. The results of the wavelet analysis presented here illustrate how chl a responds to this mesoscale variability in the physical environment. Peaks in the latitudinal distribution of chl a variance in the 100- to 200-day period band (Figures 3e−3h) occur consistently at certain locations (46°N−49°N, 44°N, 43°N, 40°N−42°N, 36°N−38°N and 35°N). These maxima are localized and discrete, with distinct minima separating them. Where minima occur, chl a variance is low at all periods (Figure 4). Several of the chl a variance peaks correspond to the location of coastal capes and promontories, suggesting an association with the coastline topography.

[15] The broad peak between ~46°N and 49°N, corresponding to the Washington coast and Vancouver Island, occurs in all transects. Isolated eddies and large-scale meanders in the coastal current off Vancouver Island have frequently been observed in satellite SST imagery [*Mysak*, 1977; *Ikeda et al.*, 1984a, 1984b; *Thomson and Emery*, 1988; *Thomson and Gower*, 1998]. The abrupt change in the width of the shelf, existence of submarine canyons, or baroclinic instability in the alongshore flow have all been hypothesized to cause the observed variability [*Freeland and Denman*, 1982; *Thomson*, 1984; *Willmott and Thomson*, 1994]. Greater than 20 km offshore the peak chl a variance in this region occurs at ~48.5°N, coincident with the Juan de Fuca strait. A recurrent eddy forms
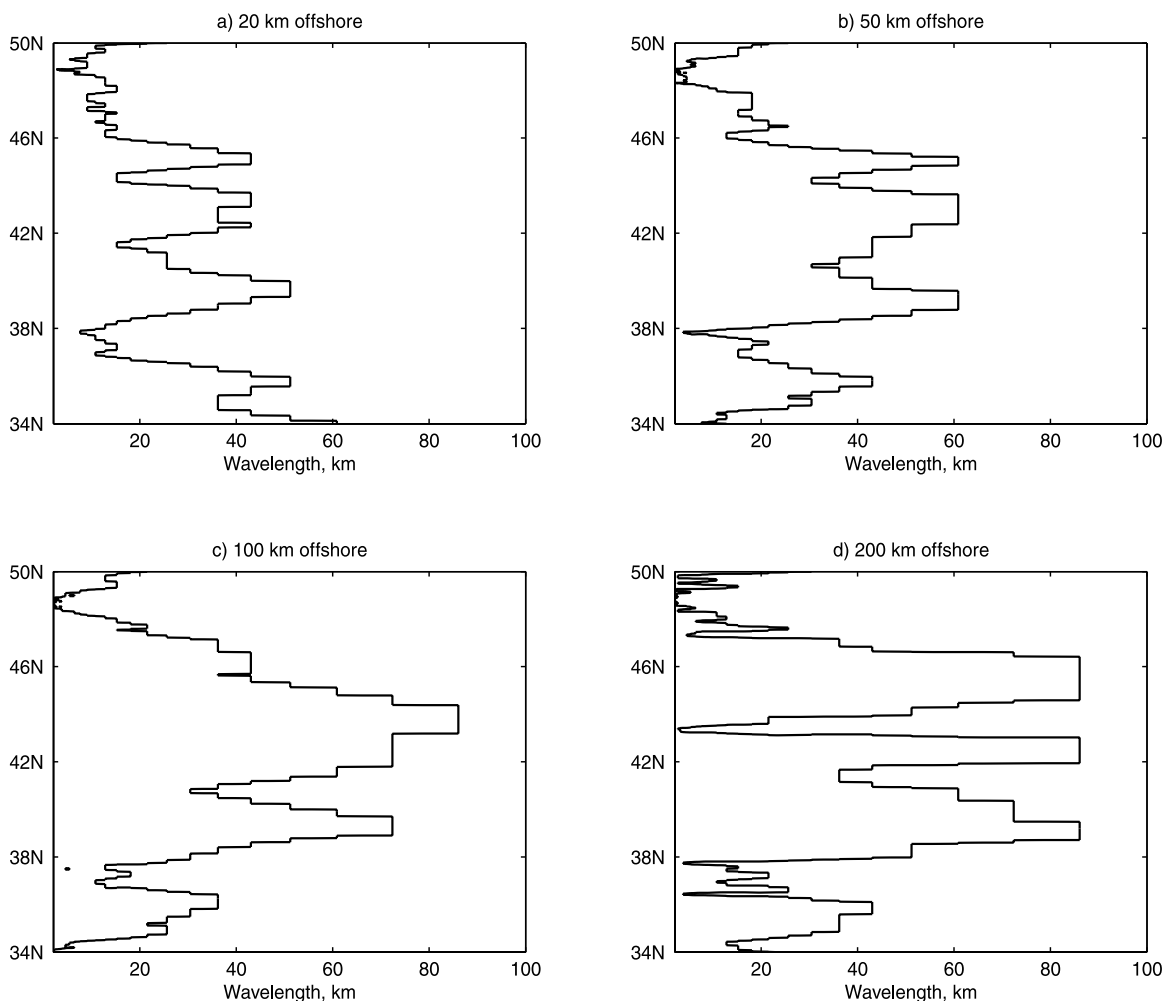
Figure 5. Shortest statistically significant (95% level) wavelength plotted as a function of latitude, derived from a spatial analysis of time-mean chl *a* transects taken (a) 20 km, (b) 50 km, (c) 100 km, and (d) 200 km offshore.

annually in summer at the mouth of the strait. Its influence, reflected in SST, density and velocity structure, extends >150 km offshore [*Freeland and Denman*, 1982; *MacFadyen et al.*, 2005]. These processes which contribute variance to the physical system appear to be reflected in enhanced biological variance too.

[16] A large submarine bank, Heceta Bank, extends ∼50 km offshore between 43.8°N and 44.6°N. The bank disrupts the alongshore flow of the coastal jet, increasing its offshore excursion [*Castelao and Barth*, 2005]. A low-velocity zone is located inshore of the bank, resulting in retention of water and accumulation of biomass, both zooplankton and phytoplankton [*Barth et al.*, 2005]. We find a narrow peak in chl *a* variance at ∼44°N in the two nearshore transects (20 and 50 km offshore). At 100 km offshore the peak is much smaller and not well separated from neighboring peaks, and at 200 km offshore the clear peak has vanished altogether. Chl *a* variance is increased nearshore on the downstream edge of Heceta Bank, but not offshore of the 200-m isobath (which lies ∼70 km offshore here).

[17] Cape Blanco (∼43°N) separates a region to the north where the coastal jet lies close to the shore, from a

region to the south where the jet meanders well offshore of the shelf [*Barth et al.*, 2000]. The flow-topography inter-action and locally intensified wind speed and wind stress curl downwind of Cape Blanco [*Samelson et al.*, 2002; *Perlin et al.*, 2004] greatly increases the mesoscale activity downstream (i.e., south) of the Cape, where more convo-luted fronts are observed in SST imagery [*Castelao and Barth*, 2005]. At the Cape itself (i.e., at 43°N) chl *a* variance is at a minimum, but a broad maximum occurs between ∼40°N and 42°N, up to ∼100 km offshore (Figures 3e–3h). This is consistent with the increased mesoscale variability observed downstream of the cape. Here again, a region of increased variance in physical parameters is also expressed as increased chl *a* variance.

[18] The chl *a* variance remains elevated until just south of Cape Mendocino, at ∼40.5°N (Figure 3). Here the peak in chl *a* variance occurs coincident with the cape, rather than downstream of it. Variance decreases sharply between ∼38°N and 40°N, reaching its nadir at ∼39°N, coincident with Point Arena. The region between Cape Mendocino and Point Arena has very low chl *a* variability <100 km offshore. Farther offshore variance is low, although not at a minimum.

[19] A broad peak in chl *a* variance is located at each distance offshore between 36°N and 38°N, downstream of Point Arena (Figures 3e–3h). The region south of the Point has been identified as an area of high eddy kinetic energy [*White et al.*, 1990; *Batteen and Vance*, 1998; *Strub and James*, 2000]. The southward meandering jet is deflected offshore again at Point Arena, but does not return inshore as strongly as farther north [e.g., *Brink et al.*, 2000]. South of Point Arena, conditions become more characteristic of a 'field of mesoscale eddies' [*Strub et al.*, 1990]. Wind stress curl also reaches a maximum southwest of Point Arena, due to the orographic intensification of the wind around the cape [*Enriquez and Friehe*, 1995; *Tjernström and Grisogono*, 2000; *Perlin et al.*, 2004]. The latitudinal distribution of chl *a* variance at Point Arena is similar to that seen at Cape Blanco. At the cape itself, variance is low but is greatly enhanced downstream of it.

[20] Chl *a* variance decreases between ∼35°N and 36°N, but starts to increase again south of Point Conception (34.5°N), suggesting that variance is also enhanced downstream of this cape. However, our study area ends at 34°N and results at the boundaries must be viewed with caution owing to edge effects.

[21] In the CCS, the role of topographic features in perturbing the southward-flowing coastal jet and promoting mesoscale meanders and eddies has been frequently studied in modeled and satellite SST and altimetric data [*Ikeda and Emery*, 1984a, 1984b; *Haidvogel et al.*, 1991; *Batteen*, 1997; *Barth et al.*, 2000; *Batteen et al.*, 2003; *Marchesiello et al.*, 2003; *Castelao and Barth*, 2005]. It remains unclear the extent to which the meanders in the coastal jet are caused by the physical presence of the capes themselves, or by inherent baroclinic or barotropic instabilities in the flow. Regardless of the mechanism, the capes and promontories of the California Current System clearly enhance the physical variability of the region. Our results quantify the enhanced biological variability, associated with increased physical variability, downstream of the capes.

4.2. Wavelength Scales

[22] In Figures 3a–3d relatively regularly spaced peaks in chl *a* variance are frequently observed, for example, in 1999 at 100 km offshore or in 2001 at 50 km offshore. These maxima are spaced ∼50–150 km apart. In the northern CCS, satellite imagery of SST shows meanders spaced ∼120–150 km apart [*Ikeda et al.*, 1984a]. The authors suggested that the spacing of capes in the region matched the wavelength of inherent baroclinic instabilities in the coastal jet, enhancing their growth into large-scale meanders. Some of the peaks in chl *a* variance we observe are of this order, but many are more closely spaced. These may be due to finer-scale mesoscale variability, such as filaments or offshoots associated with the larger-scale meanders.

[23] The wavelengths of mesoscale features observed in SST data have been estimated to be from ∼60–150 km (from shortest to longest: *Denman and Freeland* [1985], *Mysak* [1977], *Thomson* [1984], *Ikeda et al.* [1984b], *Wright* [1980], and *Emery and Mysak* [1980]). This is a little longer than the 30–120 km we estimated as the dominant wavelengths in chl *a* (from wavelet analysis of data at individual times, not shown). In the time-mean analysis, the shortest statistically significant wavelengths

vary from ∼5 to 90 km (Figure 5) and have a latitudinal distribution similar to that observed in chl *a* variance (Figures 3e–3h). The smallest significant wavelengths decrease from ∼50 km to ∼10 km at 47°N–50°N (off Vancouver Island), ∼44°N (in the vicinity of Heceta Bank), 40°N–42°N (downstream of Cape Blanco) and 36°N–38°N (downstream of Point Arena). These are the same locations at which increased chl *a* variance is observed.

[24] As noted by *Lévy and Klein* [2004], deformation of a flow will result in a cascade of energy that generates small-scale variability in the large-scale pattern. Our results suggest that the coastal topography increases variance in the chlorophyll concentration, and also transfers energy into smaller-scale variability.

4.3. Relationship to Physical Variability

[25] To assess the correspondence between latitudinal patterns of chl *a* variance and physical processes, transects of sea level anomaly (SLA) at the same distances offshore as the chl *a* transects (20, 50, 100 and 200 km) were constructed and temporal variance calculated at each location. SLA variance and chl *a* variance in the 100- to 200-day period band are plotted together as a function of latitude in Figure 6. In the nearshore locations (20 and 50 km offshore) there is remarkable coherence between the latitudinal distribution of SLA and chl *a* variance suggesting strong Lagrangian control of biological variability by physical processes. Peaks in SLA variance occur off Washington/Vancouver Island (46°N–50°N), at Heceta Bank (∼44°N) and downstream of Cape Blanco and Point Arena (43°N and 39°N, respectively). At 100 km offshore, peaks in chl *a* and SLA variance still coincide in the north (46°N–50°N) and the south (34°N–38°N) of the region, but not in the central area. By 200 km offshore, there appears to be almost no correspondence between latitudinal patterns of SLA and chl *a* variance. This could arise because biological variability at this distance offshore is expressed primarily in a subsurface chlorophyll maximum [e.g., *Cullen and Eppley*, 1981; *Millan-Nunez et al.*, 1997] which cannot be observed by the satellite. Alternatively, the disconnect between SLA and chl *a* > 100 km offshore suggests that different processes control their distributions and that phytoplankton do not act as passive tracers throughout the region. Unlike the chl *a*, variance in SLA is not reduced farther offshore, indicating that physical mesoscale variability is still occurring. However, the dissimilarity between the SLA and chl *a* profiles suggests that chl *a* is no longer responding in the same way as closer to shore.

[26] Chlorophyll may act as a passive tracer of physical processes in the nearshore CCS region [*Abbott and Zion*, 1985; *Denman and Abbott*, 1988, 1994; *Smith et al.*, 1988]. Spectral analysis of satellite SST and phytoplankton pigment data suggest that <200 km offshore, chl *a* and SST are closely linked and respond to similar physical forcing [*Abbott and Letelier*, 1998]. Farther offshore, however, the timescales of SST and chlorophyll diverge, indicating control by different processes.

[27] There is ongoing debate concerning the extent to which the distribution of phytoplankton is controlled by physical or biological processes (see *Martin* [2003] for a review). In physically dynamic regions such as the CCS, it has been suggested that biological processes such as predation or competition are less important than physical forcing
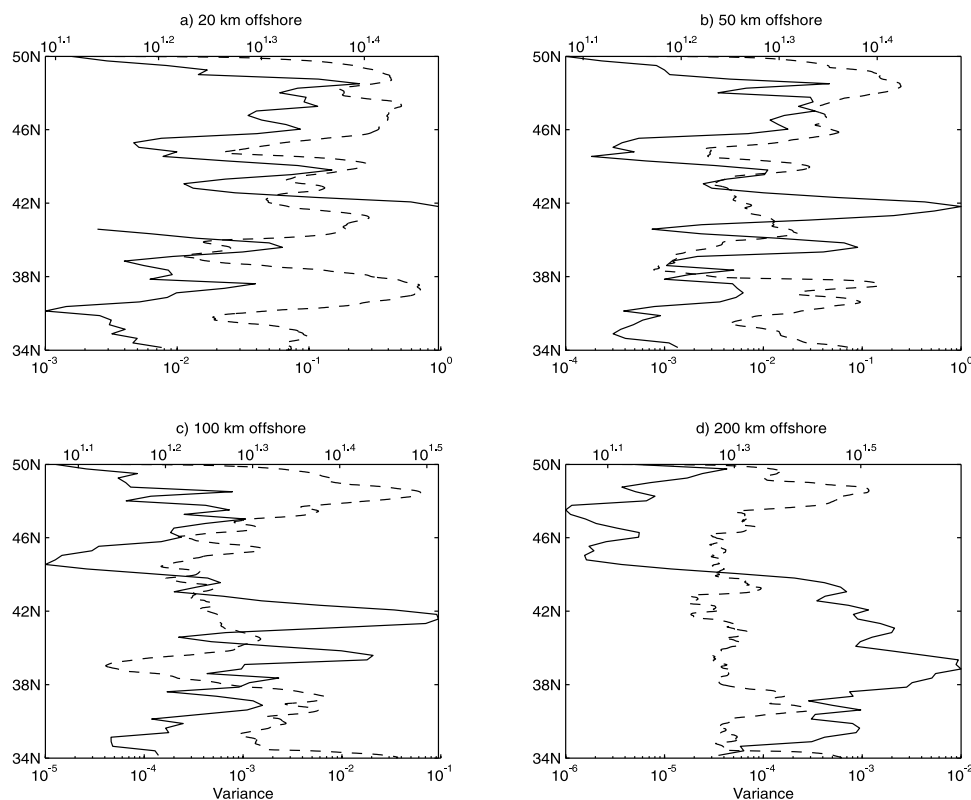
Figure 6. Variance in sea level anomaly (solid line, cm^2, upper axis) and chl a in the 100- to 200-day period band (dashed line $(mg\ m^{-3})^2$, lower axis) plotted as a function of latitude for transects taken (a) 20 km, (b) 50 km, (c) 100 km, and (d) 200 km offshore.

for determining the spatial distribution of phytoplankton [*McGowan and Walker*, 1985]. More recently, however, it has been made clear that the physical versus biological control of plankton patchiness depends on the scales at which observations are made [*Franks*, 2005]. Our results suggest that at seasonal timescales (periods of ∼100–200 days), the same processes determine the latitudinal distribution of both phytoplankton and the physical environment in the nearshore region (<100 km offshore). Farther offshore, the surface physical and biological patterns are no longer in synchrony, suggesting control by different forcing mechanisms, i.e., a shift from physical to biological control of the chl a distribution [*Denman and Abbott*, 1994; *Abbott and Letelier*, 1998].

5. Summary

[28] The application of wavelet analysis to the SeaWiFS data set affords a unique perspective on the scales of variability in chlorophyll concentration in the CCS. In this paper we examine the spatial distribution of SeaWiFS chl a variance. Dominant temporal scales and interannual variability are discussed in a companion paper (HT07). Chl a scales of variability are similar to those seen in sea level anomaly, and have a similar spatial and temporal distribution, providing indirect evidence of the influence of mesoscale variability on phytoplankton populations.

[29] The latitudinal distribution of chlorophyll variance in the CCS corresponds closely to features of the coastal topography. Peaks in variance are found offshore of Vancouver Island and downstream of Heceta Bank, Cape Blanco, Point Arena and possibly Point Conception. Shorter-wavelength variability occurs in the same locations as increased chl a variance, suggesting that the coastal topography of the CCS not only enhances biological variability, but also results in smaller mesoscale features. The latitudinal distribution of SLA variance is very similar to chl a in the nearshore region (<100 km offshore); however farther offshore there is no correspondence between SLA and chl a variance. This suggests a transition from physical to biological control of the chlorophyll distribution.

[30] Wavelet analysis is a promising and versatile technique for investigating dominant scales of variability that has not yet been widely used in oceanographic applications. In part this may be because a long data set (relative to the sampling frequency) is needed. However, this makes it ideal for investigating satellite data, or records from moorings, buoys or floats: cases where the amount of data can be overwhelming. Results presented here quantify the latitudinal and cross-shelf distribution of the dominant temporal scales of phytoplankton variability in the California Current System.

References

Abbott, M. R., and B. Barksdale (1991), Phytoplankton pigment patterns and wind forcing off central California, *J. Geophys. Res.*, *96*(C8), 14,649–14,667.

Abbott, M. R., and R. M. Letelier (1998), Decorrelation scales of chlorophyll as observed from bio-optical drifters in the California Current, *Deep Sea Res., Part II*, *45*(8–9), 1639–1667.

Abbott, M. R., and P. M. Zion (1985), Satellite observations of phytoplankton variability during an upwelling event, *Cont. Shelf Res.*, *4*(6), 661–680.

Barth, J. A., S. D. Pierce, and R. L. Smith (2000), A separating coastal upwelling jet at Cape Blanco, Oregon and its connection to the California Current System, *Deep Sea Res., Part II*, *47*(5–6), 783–810.

Barth, J. A., S. D. Pierce, and T. J. Cowles (2005), Mesoscale structure and its seasonal evolution in the northern California Current System, *Deep Sea Res., Part II*, *52*(1–2), 5–28.

Batteen, M. L. (1997), Wind forcing modeling studies of currents, meanders and eddies in the California Current system, *J. Geophys. Res.*, *102*(C1), 985–1010.

Batteen, M. L., and P. W. Vance (1998), Modeling studies of the effects of wind forcing and thermohaline gradients on the California Current System, *Deep Sea Res., Part II*, *45*(8–9), 1507–1556.

Batteen, M. L., N. J. Cipriano, and J. T. Monroe (2003), A large-scale seasonal modeling study of the California Current System, *J. Oceanogr.*, *59*(5), 545–562.

Brink, K. H., R. C. Beardsley, J. Paduan, R. Limeburner, M. Caruso, and J. G. Sires (2000), A view of the 1993–1994 California Current based on surface drifters, floats and remotely sensed data, *J. Geophys. Res.*, *105*(C4), 8575–8604.

Castelao, R. M., and J. A. Barth (2005), Coastal ocean response to summer upwelling favorable winds in a region of alongshore bottom topography variations off Oregon, *J. Geophys. Res.*, *110*, C10S04, doi:10.1029/2004JC002409.

Chavez, F. P., R. T. Barber, P. M. Kosro, A. Huyer, S. R. Ramp, T. P. Stanton, and B. R. Demendiola (1991), Horizontal transport and the distribution of nutrients in the coastal transition zone off Northern California: Effects on primary production, phytoplankton biomass and species composition, *J. Geophys. Res.*, *96*(C8), 14,833–14,848.

Cullen, J. J., and R. W. Eppley (1981), Chlorophyll maximum layers of the Southern California Bight and possible mechanisms of their formation and maintenance, *Oceanol. Acta*, *4*(1), 23–32.

Daubechies, I. (1992), *Ten Lectures on Wavelet Analysis*, 357 pp., Soc. for Ind. and Appl. Math., Philadelphia, Pa.

Denman, K. L., and M. R. Abbott (1988), Time evolution of surface chlorophyll patterns from cross-spectrum analysis of satellite color images, *J. Geophys. Res.*, *93*(C6), 6789–6798.

Denman, K. L., and M. R. Abbott (1994), Time scales of pattern evolution from cross-spectrum analysis of advanced very high-resolution radiometer and coastal zone color scanner imagery, *J. Geophys. Res.*, *99*(C4), 7433–7442.

Denman, K. L., and H. J. Freeland (1985), Correlation scales, objective mapping and a statistical test of geostrophy over the continental shelf, *J. Mar. Res.*, *43*(3), 517–539.

Emery, W. J., and L. A. Mysak (1980), Dynamical interpretation of satellite-sensed thermal features of Vancouver Island, *J. Phys. Oceanogr.*, *10*(6), 961–970.

Enriquez, A. G., and C. A. Friehe (1995), Effects of wind stress and wind stress curl variability on coastal upwelling, *J. Phys. Oceanogr.*, *25*(7), 1651–1671.

Franks, P. J. S. (2005), Plankton patchiness, turbulent transport and spatial spectra, *Mar. Ecol. Prog. Ser.*, *294*, 295–309.

Freeland, H. J., and K. L. Denman (1982), A topographically controlled upwelling center off southern Vancouver Island, *J. Mar. Res.*, *40*(4), 1069–1093.

Haidvogel, D. B., A. Beckmann, and K. S. Hedstrom (1991), Dynamic simulations of filament formation and evolution in the coastal transition zone, *J. Geophys. Res.*, *96*(C8), 15,017–15,040.

Henson, S. A., and A. C. Thomas (2007), Phytoplankton scales of variability in the California Current System: 1. Interannual and cross-shelf variability, *J. Geophys. Res.*, *112*, C07017, doi:10.1029/2006JC004039.

Hickey, B. M. (1979), The California Current System—Hypotheses and facts, *Prog. Oceanogr.*, *8*(4), 191–279.

Hickey, B. M. (1998), Coastal oceanography of western North America from the tip of Baja California to Vancouver Island, in *The Sea*, vol. 11, edited by A. R. Robinson and K. H. Brink, pp. 345–395, John Wiley, Hoboken, N. J.

Huyer, A., J. H. Fleischbein, J. Keister, P. M. Kosro, N. Perlin, R. L. Smith, and P. A. Wheeler (2005), Two coastal upwelling domains in the northern California Current system, *J. Mar. Res.*, *63*(5), 901–929.

Ikeda, M., and W. J. Emery (1984a), Satellite observations and modeling of meanders in the California Current System off Oregon and Northern California, *J. Phys. Oceanogr.*, *14*(9), 1434–1450.

Ikeda, M., and W. J. Emery (1984b), A continental shelf upwelling event off Vancouver Island as revealed by satellite infrared imagery, *J. Mar. Res.*, *42*(2), 303–317.

Ikeda, M., W. J. Emery, and L. A. Mysak (1984a), Seasonal variability in meanders of the California Current system off Vancouver Island, *J. Geophys. Res.*, *89*(C3), 3487–3505.

Ikeda, M., L. A. Mysak, and W. J. Emery (1984b), Observation and modeling of satellite-sensed meanders and eddies off Vancouver Island, *J. Phys. Oceanogr.*, *14*(1), 3–21.

Lévy, M. L., and P. Klein (2004), Does the low frequency variability of mesoscale dynamics explain a part of the phytoplankton and zooplankton spectral variability?, *Proc. R. Soc., Ser. A*, *460*(2046), 1673–1687.

MacFadyen, A., B. M. Hickey, and M. G. G. Foreman (2005), Transport of surface waters from the Juan de Fuca eddy region to the Washington coast, *Cont. Shelf Res.*, *25*(16), 2008–2021.

Mackas, D. L., L. Washburn, and S. L. Smith (1991), Zooplankton community pattern associated with a California Current cold filament, *J. Geophys. Res.*, *96*(C8), 14,781–14,797.

Marchesiello, P., J. C. McWilliams, and A. Shchepetkin (2003), Equilibrium structure and dynamics of the California Current System, *J. Phys. Oceanogr.*, *33*(4), 753–783.

Martin, A. P. (2003), Phytoplankton patchiness: The role of lateral stirring and mixing, *Prog. Oceanogr.*, *57*(2), 125–174.

McGowan, J. A., and P. W. Walker (1985), Dominance and diversity maintenance in an oceanic ecosystem, *Ecol. Monogr.*, *55*, 103–118.

Millan-Nunez, R., S. Alvarez-Borrego, and C. C. Trees (1997), Modeling the vertical distribution of chlorophyll in the California Current System, *J. Geophys. Res.*, *102*(C4), 8587–8595.

Morlet, J. (1983), Sampling theory and wave propagation, in *Issues on Acoustic Signal/Image Processing and Recognition*, *NATO ASI Ser.*, vol. 1, edited by C. H. Chen, pp. 233–261, Springer, Berlin.

Mysak, L. A. (1977), Stability of California undercurrent off Vancouver Island, *J. Phys. Oceanogr.*, *7*(6), 904–917.

Perlin, N., R. Samelson, and D. Chelton (2004), Scatterometer and model wind and wind stress in the Oregon-northern California coastal zone, *Mon. Weather Rev.*, *132*(8), 2110–2129.

Ramp, S. R., P. F. Jessen, K. H. Brink, P. P. Niiler, F. L. Daggett, and J. S. Best (1991), The physical structure of cold filaments near Point Arena, California, during June 1987, *J. Geophys. Res.*, *96*(C8), 14,859–14,883.

Samelson, R., P. Barbour, J. A. Barth, S. Bielli, T. Boyd, D. Chelton, P. M. Kosro, M. Levine, E. Skyllingstad, and J. Wilczak (2002), Wind stress forcing of the Oregon coastal ocean during the 1999 upwelling season, *J. Geophys. Res.*, *107*(C5), 3034, doi:10.1029/2001JC000900.

Smith, R. C., X. Y. Zhang, and J. Michaelsen (1988), Variability of pigment biomass in the California Current System as determined by satellite imagery: 1. Spatial variability, *J. Geophys. Res.*, *93*(D9), 10,863–10,882.

Strub, P. T., and C. James (2000), Altimeter-derived variability of surface velocities in the California Current System: 2. Seasonal circulation and eddy statistics, *Deep Sea Res., Part II*, *47*(5–6), 831–870.

Strub, P. T., C. James, A. C. Thomas, and M. R. Abbott (1990), Seasonal and nonseasonal variability of satellite-derived surface pigment concentration in the California Current, *J. Geophys. Res.*, *95*(C8), 11,501–11,530.

Thomson, R. E. (1984), A cyclonic eddy over the continental margin of Vancouver Island—Evidence for baroclinic instability, *J. Phys. Oceanogr.*, *14*(8), 1326–1348.

Thomson, R. E., and W. J. Emery (1988), Relationships between near-surface plankton concentrations, hydrography and satellite measured sea surface temperature, *J. Geophys. Res.*, *93*(C12), 15.733–15.738.

Thomson, R. E., and J. F. R. Gower (1998), A basin-scale oceanic instability event in the Gulf of Alaska, *J. Geophys. Res.*, *103*(C2), 3033–3040.

Tjernstrom, M., and B. Grisogono (2000), Simulations of supercritical flow around points and capes in a coastal atmosphere, *J. Atmos. Sci.*, *57*(1), 108–135.

Torrence, C., and G. P. Compo (1998), A practical guide to wavelet analysis, *Bull. Am. Meteorol. Soc.*, *79*(1), 61–78.

Traganza, E. D., D. A. Nestor, and A. K. McDonald (1980), Satellite observations of a nutrient upwelling off the coast of California, *J. Geophys. Res.*, *85*(C7), 4101–4106.

Washburn, L., D. C. Kadko, B. H. Jones, T. Hayward, P. M. Kosro, T. P. Stanton, S. R. Ramp, and T. Cowles (1991), Water mass subduction and the transport of phytoplankton in a coastal upwelling system, *J. Geophys. Res.*, *96*(C8), 14,927–14,945.

White, W. B., C. K. Tai, and J. Dimento (1990), Annual Rossby wave characteristics in the California Current region from the Geosat exact repeat mission, *J. Phys. Oceanogr.*, *20*(9), 1297–1310.

Willmott, A. J., and R. E. Thomson (1994), Forced shelf wave dynamics for a discontinuous shelf width—Application to Vancouver Island, *J. Phys. Oceanogr.*, *24*(6), 1347–1367.

Wright, D. G. (1980), On the stability of a fluid with specialized density stratification. 2. Mixed barocline-barotropic instability with application to the northeast Pacific, *J. Phys. Oceanogr.*, *10*(9), 1307–1322.

————————————
S. A. Henson and A. C. Thomas, School of Marine Sciences, University of Maine, Orono, ME 04469, USA. (stephanie.henson@umit.maine.edu)